Domain Wall Dynamics for a 1D Bose gas

Léa Dubois[1], G. Themèze, J. Dubail and I. Bouchoule,

1 Laboratoire Charles Fabry, Institut d'Optique, Université Paris-Saclay
⋆ lea.dubois@universite-paris-saclay.fr

December 12, 2024

Abstract

Abstract

Contents

List of figures :

- For the experimental setup : atom chip with the shape of the longituinal trap + linear density profil of the initial situation
- For the experimental data : Euler scale observed
- For the experimental data : edge profile with (T=0, Lieb-Liniger) and (T=0, GP)
- experimental edge profile + fit by GE + fit of the left part by GE + fit of the right part by GE + insert avec fig. 9.9 de la thèse de Léa **enlever les ajustements thermiques gauches et droites**
- (a) experimental edge profile + fit by function s (4 fittng parameters) ; (b) distribution des facteurs d'occupation (c) distributions de rapidités
- local rapdity distribution : voir dernière figure déjà mise

1 Introduction

Gaining insight on the out-of-equilibrium dynamics of many-body quantum systems is tremendously difficult and it is the goal of an active research field. One particular class of systems where important progress have been done is the class of integrable one-dimensional systems. Owing to their infinite number of local conserved charges, to describe the local properties of equilibrium states that arise after relaxation, one needs a whole function, the rapidity distribution[ ]. The latter can be viewed as the distribution in velocity space of the infinite-lifetime quasi-particles in the system. Large scale dynamics is accounted for by a generalized hydrodynamic (GHD) effective theory[ ], which assume local equilibrium. A paradigmatic situation that can be handled by this theory is the dynamics induced by a partite quench [1,2], dubbed domain-wall protocol in this paper. In this protocol the Hamiltonian governing the dynamic is translation invariant but the initial state is the junction of two semi-infinite homogeneous systems each prepared in a different equilibrium state from the Hamiltonian. The GHD theory predicts that, at time long enough such that diffusion effects become negligible [3] and Euler-scale hydrodynamics is valid, the time evolution is ballistic. An interesting feature of this protocol is that the local state, within the merging region, is expected to present features characteristic of zero-temperature systems. Thus, this protocol could be used to reveal power-law singularities of correlation function characteristic of zero-temperature Luttinger liquid [4], providing a local probe is performed.

In this paper, we experimentally realize an instance of the domain-wall protocol using an ultra-cold atomic Bose gas, well described by the Lieb-Liniger model of one-dimensional Bosons with contact repulsive interactions [5,6], which is an integrable model. The domain wall consists in our experiment in the junction of a gas prepared in an equilibrium state on the one side, and the vacuum on this other side. It is prepared, starting from a homogeneous cloud, by the sudden removal of its left part. For different evolution times, we record the density profile of the border between the two zones, dubbed the border profile. We find that the border profile shows a ballistic behavior, as expected from GHD theory at Euler scale.

The border profile, for clouds prepared with deep evaporative cooling, is in fair agreement with GHD predictions assuming the semi-infinite gas is in its ground state, although deviations are present. We show that, from the border profile, it is in principle possible to reconstruct the rapidity distribution characterizing the initial gas. This protocol can thus be used as a generalized thermometry. However, the reconstruction method suffers from a high sensitivity to experimental noise in the tail of the border profile, which prevent us to reconstruct faithfully the initial rapidity distribution. Instead, we use an ansatz parametrized by a few parameters to extract the rapidity distributions of the initial gas from a fit to the border profile.

Finally, we use a newly developed techniques [7] to probe the local rapidity distribution within the border. The latter is expected to be highly asymmetric for an initial state whose rapidity distribution is substantially broader and smoother than that of the ground state: while one of its border reflects the broad character of the initial rapidity distribution, the other border present the sharp feature expected for the ground state. Our experimental data show such an asymmetric behavior, although the above feature is softened by the finite spatial resolution of the local rapidity distribution measurement.

2 Experimental setup

We produce an ultra-cold gas of ^{87}Rb bosonic atoms in the stretched state $|F = 2, m_F = 2\rangle$ using an atom chip. In addition to a homogeneous longitudinal magnetic field $B_0 = 3.36$G, transverse trapping is achieved with three parallel microwires deposited on the chip (shown in blue

in Fig.1(a)) which carry AC currents at 400MHz. This configuration eliminates wire roughness effects and allows independent control over both longitudinal and transverse confinement [8]. The atoms are trapped 7μm from the chip surface and 15μm from the wires, enabling strong transverse confinement. The transverse trapping potential used in the following is harmonic, with a frequency of $\omega_\perp/2\pi = 2.56$kHz. Using radio-frequency evaporative cooling, we produce an atomic cloud at a temperature of approximately $T = 100$nK and a chemical potential of $\mu/k_B = 45$nK. With these parameters, $\mu/(\hbar\omega_\perp) = 0.4$ and $k_BT/(\hbar\omega_\perp) = 0.8$, the gas enters in the 1D regime. The effective 1D coupling constant for atoms in the transverse ground state is given by $g = 2a_{3D}\hbar\omega_\perp$ where a_{3D} is the 3D scattering length of ^{87}Rb [9]. Further details on the setup can be found in **REF**.

The longitudinal magnetic trap is produced by DC currents through four wires positioned on either side of the three microwires, as shown in the Fig.1(a). Since these wires are placed far from the center of the chip, the longitudinal potential can be expressed as a polynomial series expansion $V(x) = \sum_i a_i x^i$. The fourth first coefficients a_i are tuned by adjusting the currents in the four wires that generate the longitudinal trapping potential. By carefully selecting these currents, it is possible to set a_1, a_2 and a_3 to zero. Since the higher-order coefficients $\{a_i\}_{i>4}$ can be neglected, setting a_1, a_2, and a_3 to zero produces as a first appxoimation a quartic potential. This potential shape is particularly useful in our case: to experimentally study domain wall dynamics in 1D Bose gases, it is important to achieve a quasi-homogeneous atomic density over a relatively large region. The quartic potential satisfies these requirements. An example of linear density extracted from an atomic cloud placed in such a potential is represented in gray in Fig.1(b). The linear density n_0 remains constant to within 10% around the peak density over a range of approximately 250μm.

With a near-zero dimensionless Lieb parameter $\gamma = mg/(\hbar^2 n_0) \in [0.4, 0.7] \times 10^{-2}$ and a temperature $T \ll n_0^{3/2}\sqrt{\hbar^2 g/m}/k_B$, the atomic clouds produced are deeply in the quasi-condensate regime, where density fluctuations are almost completely suppressed, but phase fluctuations remain [10].

To produce an initially semi-infinite homogeneous gas, we use the selection method introduced in [11]. We illuminate an edge of the atomic cloud, initially in equilibrium in a quartic trap, with light that is nearly resonant with the $F = 2 \rightarrow F' = 3$ transition of the $D2$ line. Atoms shined by this light are subjected to radiation pressure : after being illuminated for 30μs corresponding to ~ 15 absorption/reemission cycles, they are no longer trapped. To illuminate only an edge of the gas, the beam is shaped using a digital micromirror device (DMD). Further details on this spatial selection method are available in [11]. This protocol produces a clean edge between a zero density system and a homogeneous gas due to the fact that the atoms are initially placed in a quartic trap. An example of the density profile of a gas initially in equilibrium in a quartic trap, after applying this spatial selection tool, is shown in yellow in Fig.1(b). The gas is then homogeneous to within 10% over a distance of approximately 200μm.

The longitudinal confinement is then removed while maintaining the transverse confinement. The initial sharp border braodends in time and this dynamics is monitored by recording longitudinal density profiles $n(x,t)$ after different evolution time t.

3 GHD predictions

Under time evolution, the initial sharp border of the cloud smoothens, and the time derivative of local quantities decrease. After some time, upon coarse graining in position and time, one expects that the gas can locally be described by equilibrium states. Equilibrium states of the Lieb-Liniger model are entirely characterized by their rapidity distribution $\rho(\theta)$. Equivalently,

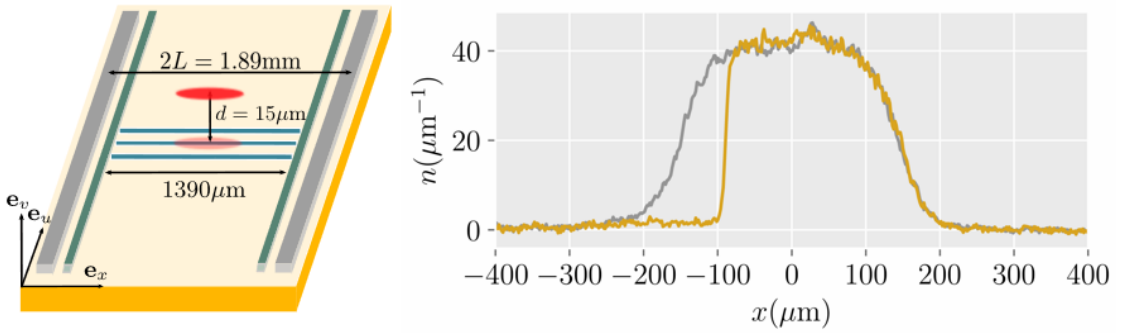

Figure 1: (a) Schematic drawing of the atom chip. The 3 blue wires produce the transverse trapping, the 4 other wires produce the longitudinal trapping. The red oval ball represents the atomic cloud, trapped 15 microns above the wires – (b) The gray curve represents the linear density profile of gas confined within a quartic potential. The atomic cloud is then illuminated during $30\mu s$ by a near resonant light beam, shaped using a DMD. The resulting density profile is depicted in yellow.

equilibrium states can be parametrized by a function $\nu(x,t,\theta)$ dubbed the occupation factor which takes values between 0 and 1 and which is related to ρ by $\nu(\theta) = \rho(\theta)/\rho_s(\theta)$, where $\rho_s(\theta) = 1/(2\pi)\left(1 + \int d\theta' \Delta(\theta-\theta')\rho(\theta')\right)$ and the function Δ is $\Delta(\Theta) = 2g/(g^2/\hbar + \hbar\Theta^2)$. The functions ν and ρ are in one-to-one correspondence and in the following we use either ρ or ν. Since local equilibrium is assumed, the system as a whole is described by a time- and position-dependent rapidity distribution $\rho(x,t,\theta)$, or equivalently by the time- and position-dependent occupation factor $\nu(x,t,\theta)$. The latter leads to simpler calculations, while the former is particularly useful to extract the linear density, which reads $n(x,t) = \int d\theta\, \rho(x,t,\theta)$.

The GHD theory provides a prediction for $\rho(x,t,\theta)$, or equivalently for $\nu(x,t,\theta)$. At large enough length scales, it reduces to its Euler-Scale approximation which, written in terms of ν, takes the convective form

$$\frac{\partial \nu}{\partial t} + v^{\text{eff}}_{[\nu]}\frac{\partial \nu}{\partial x} = 0 \tag{1}$$

where the effective velocity $v^{\text{eff}}_{[\nu]}$ is a functional of the local rapidity distribution which fulfills, for any rapidity θ, $v^{\text{eff}}_{[\nu]}(\theta) = \theta - \int \frac{d\theta'}{2\pi}\Delta(\theta-\theta'')\rho(\theta')\left(v_{\text{eff}}(\theta) - v_{\text{eff}}(\theta')\right)$. For an initial domain-wall state whose discontinuity is located on $x = 0$, the solution of (1) is invariant along rays of constant velocity x/t and we introduce the occupation factor distribution of the rays $\nu^*(v,\theta)$ such that

$$\nu(x,t,\theta) = \nu^*(x/t,\theta). \tag{2}$$

This equation implies that all local properties of the gas depend on x and t only through the quantity $v = x/t$. For the domain wall situation considered in this paper with, initially, a vacuum state for negative x and a state of occupation factor distribution ν_0 one the right, the function $\nu^*(v,\theta)$ is parametrized by an edge rapidity θ^* according to

$$\nu^*(v,\theta) = \begin{cases} \nu_0(\theta) \text{ if } \theta < \theta^* \\ 0 \text{ if } \theta > \theta^* \end{cases} \quad \text{where } v^{\text{eff}}_{[\nu^*]}(\theta^*) = v. \tag{3}$$

This equations can be solved numerically if the initial distribution $\nu_0(\theta)$ is known. Together with Eq.(**??**), it entirely describes the system after the Euler-scale has been reached. Note that to compute the linear density $n(x,t)$ in order to compare to experiments, one uses the relation $n(x,t) = \int d\theta \rho(x,t,\theta)$, such that the rapidity distribution needs to be computed from the knowledge of $\nu(x,t,\theta)$.

Solution for a system initially in the ground state. As an example, let us derive some implications of the above equations in the case the initial state is the ground state. The initial occupation factor distribution is then a Fermi sea. More precisely $\nu_0(\theta) = 1$ if $|\theta| < \theta_m$ and zero otherwise, where the Fermi radius θ_m depends on the initial linear density n_0. Some general features of the state of the system after the Euler-scale has been reached can be identified. The border has well-defined fronts both in the empty region of $x < 0$ and in the region of density n_0 for $x > 0$. In the region $x < 0$, the front is at $x/t = \theta_m$, since the effective velocity of a vanishing narrow Fermi sea is equal to its mean rapidity. The density vanishes for $x/t < -\theta_m$. In the region $x > 0$, the front is at $x/t = c$, where $c = v^{\rm eff}_{[\nu_0]}(\theta_m)$ is the speed of sound for the density n_0. For $x/t > c$, the system is not yet affected by the border deformation. Finally, for any x/t, the local state is a Fermi sea, displaced by some quantity $V(x/t)$ in rapidity space, which corresponds to a local Galilean boost of velocity $V(x/t)$. Exact solution can be derived in the two asymptotic regimes for large and small densities.

In the hard core limit $\gamma = g/n_0 \gg 1$, Eq.(3) is easily solved using the fact that, in this regime, $v^{\rm eff}(\theta) = \theta$ regardless of the occupation factor distribution. We then use Eq.(**??**) and the fact that a Fermi sea of radius θ_m corresponds to a linear density $n = m\theta_m/(\pi\hbar)$ in this regime to derive

$$n(x,t) = \frac{n_0}{2}\left(1 + \frac{x}{t}\frac{m}{\pi\hbar n_0}\right). \tag{4}$$

We recover the results expected for a gas of free fermions, as expected from the mapping of the hard-core bosons to fermions, which preserves the density [12].

In the quasi-BEC regime $\gamma = g/n_0 \ll 1$, we solve Eq. (3) using the fact in this regime that the effective velocity at the border of a Fermi sea of radius θ_m is $\theta_m/2$, in the frame where the Fermi sea is at rest. Then, using Eq.(**??**) and the fact that, in this regime, a Fermi sea of radius θ_m corresponds to a linear density $n = m\theta_m^2/(4g)$, we obtain

$$n(x,t) = \frac{n_0}{9}\left(\frac{x}{t}\frac{\hbar}{\sqrt{mgn_0}} + 2\right)^2. \tag{5}$$

We recover here the hydrodynamic predictions derived from the Gross-Pitaevski equation [13, 14], as expected since this classical field approach be a good description of the system in this regime.

4 Experimental data

The border profiles for different evolution times varying between $\tau = 10$ms and $\tau = 18$ms are shown in Fig.2 and are represented as a function of $v = x/\tau$. The profiles overlap remarkably well, showing that the Euler scale is reached within this time interval. The longitudinal dynamic after $\tau = 18$ms can't be probe due to the fact that our initial semi-homogeneous gas has a finite size. For shorter deformation times, experimental border profiles are smoother than Euler-scale GHD predictions, which might be due to the failure of Euler scale.

The measured border profile can be compared with the profile obtained assuming that we are in the ground state. Such a comparison is shown on Fig.**FIG** with the Lieb parameter $\gamma = 6.10^{-3}$. The agreements are rather good, especially in the high density part. For this value of the Lieb parameter, the profile is very similar to the parabola obtained in the quasi-BEC regime and given by Eq.(5). Significant deviations from the $\gamma \to 0$ regime occur for $\gamma > 1.5$, which lies outside the regime we are working in. The deviations from the parabola observed experimentally are mainly due to non-zero entropy effects.

From the knwoledge of the initial occupation factor distribution $\nu_0(\theta)$, one can predict a

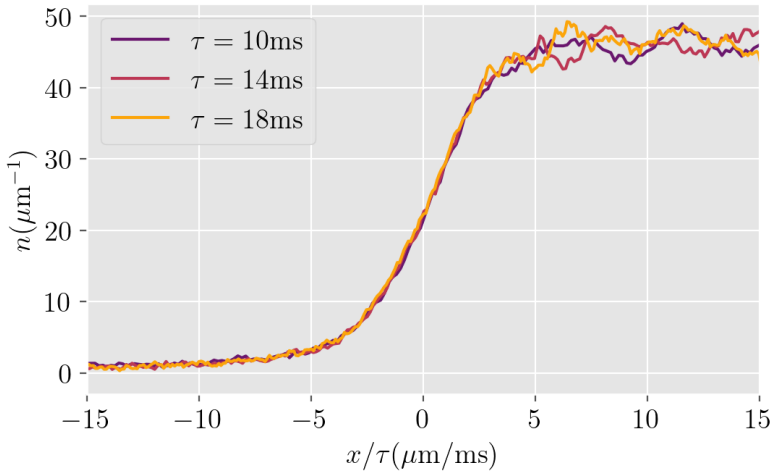

Figure 2: Caption

border profile from Euler-scale GHD. Conversely, we show below that, from a given border profile it is *a priori* possible to reconstruct the occupation factor distribution it corresponds to.

5 Extraction of the initial rapidity distribution

Here we present an attempt at reconstructing the occupation factor $\nu_0(\theta)$ in the initial state directly from the density profile $n(x/t) = n(v)$. The main idea is that the occupation factor $\nu_0(\theta)$ should satisfy a differential equation that relates it to $n(v)$. Integrating that differential equation, it is then possible to reconstruct $\nu_0(\theta)$ directly from $n(v)$.

More precisely, on parametrizes the border with the edge rapidity θ^* defined Eq. (3) and we find a pair of differential equations which write

$$\begin{cases} \dfrac{d\nu_0}{d\theta^*} = D'\dfrac{dn}{dv} + AD\dfrac{d^2n}{dv^2} \\ \dfrac{dv}{d\theta^*} = A \end{cases} \tag{6}$$

where $A(\theta^*)$ and $D(\theta^*)$, whose expressions are given in appendix, are functionnals of ν^*, *i.e.* they depend only on the value of ν_0 for $\theta < \theta^*$. Knowing the edge profile $n(v)$, and thus its derivatives dn/dv and d^2n/dv^2, one can numerically integrate the above differential equations starting from very negative value of θ^* for which $\nu_0 \simeq 0$, $A \simeq 1$, $D \simeq -2\pi$ and $v = \theta^*$. This can be done using the Euler method where, at each step, one estimates numerically D', D and A using the values of ν_0 already obtained for smaller rapidities θ^*.

This method is highly sensitive to the linear density away from the edge. Since the signal-to-noise ratio in our experimental data is poor in this region, the results obtained with this technique are not trustworthy.

We thus use an alternative method to extract the occupation factor distribution $\nu_0(\theta)$ which consists in fitting the experimental border profile with the GHD calculations based on Eq.(**??**-3). Extracting $\nu_0(\theta)$ remains unattainable it amounts to determine an infinite number of fitting parameters with a data set of finite dimension and moreover plagged by noise. We limit the number of fitting parameters choosing an ansatz for the form of the rapidity distribution.

The first ansatz that we choose is the rapidity distribution for a Gibbs ensemble, the fitting parameters being the temperature T and the chemical potential μ. The occupation factor

distribution of a thermal state is the distribution $\nu(\theta)$ which fulfills

$$s'(\nu(\theta)) = -\frac{m\theta^2}{2} + \int d\theta' \Delta(\theta - \theta') \left[s(\nu(\theta')) - \nu(\theta') s'(\nu(\theta)) \right] \tag{7}$$

where the function $s : [0 : 1] \to \mathcal{R}$ is $s(y) = \mu - k_B T \left(y \ln(y) + (1-y) \ln(1-y) \right)$ and s' is its derivative. For given T and μ, Eq. (7) is solved by iteration using the fact that the solution of $s'(\nu) = \epsilon$ is $\nu = 1/(e^{-\epsilon/(k_B T)} + 1)$. Fig. 4 shows the border density profile together with the best fit made using GHD calculations and such an ansatz for the initial occupation factor distribution. The fitted temperature and chemical potential are $T = xx$ and $\mu = xx$. The fit is quite good although we see some discrepancies: the left tail of the experimental data is wider than that of the fit while on the right side, the experimental date are more sharp. Such a behavoir is seen on all sets of data we analysed.

In an attempt to find an occupation factor distribution that lead to prediction for the border density profile fiiting better our data, we extend the previous ansatz adding a third parameter. This ansatz correspond to the function ν that solve Eq.(7) but with an s function which writes

$$s(y) = a - (b + cy) \left(y \ln(y) + (1-y) \ln(1-y) \right) \tag{8}$$

where the numbers a, b and c are fitting parameters. The case $c = 0$ corresponds to a thermal ansatz with $a = \mu$ and $b = k_B T$. A fit of our data with this ansatz gives $a/k_B = xx$nK, $b/k_B = xx$nK and $c/k_B = xx$nK. This fit decreases the square distance to the data by xx % compared to a thermal fit.

6 Probing locally the rapidity distribution

[Premier jet : Guillaume]

For an initial state whose occupation factor distribution smoothly goes to zero, such as a thermal state, the occupation factor distribution within the border, is expected to be highly asymetric according to Eq.(3): its left side shows a discontinuity similar to that of ground states while its right side shows the smooth behavior of the initial state. This implies in turn a highly asymetric rapidity local rapidity distribution. To reveal such a peculiar behavior, we use the protocol described in [7] as detailed below.

First we let the border expand for a time $t = 28\ 18^{-}$ms. To probe the rapidity distribution around $x = x_0$, we then select the slice of the gas that lies in the interval $[x_0 - \ell/2, x_0 + \ell/2]$. Finally, we let this slice expand in 1D for an expansion time τ after which we measure the longitudinal density $\tilde{n}(x, \tau)$. The latter reflects the rapidity distribution of the slice $\Pi(\theta)$, the asymptotic behavior being $\lim_{\tau \to \infty}(\tau \tilde{n}(x, \tau)) = \Pi(x/\tau)$. The asymetry of Π thus induces an asymetry of $\tilde{n}(x, \tau)$ in x. Such an asymetry is seen in the experimental profile obtained for $\tau =$ 50 (30) ms shown in Fig. (4a).

We start by fitting the edge deformation profile using GHD simulations n_{GHD}, with the temperature T as an adjustable parameter. The chemical potential μ is parameterized as a function of the temperature and the initial spatial density of the cloud, denoted n_p. μ is determined using a Yang-Yang thermal model to match the initial spatial density n_p, measured at 47 (56.6) μm^{-1}. The optimal fit for the edge deformation is obtained with a temperature $T = 966$ (559) nK and a chemical potential $\mu = 43$ (65) nK (see orange curve in Fig. 4b). Over the interval $[-220, 70]$ ($[-150, 100]$) μm, $\chi^2 = \|(n - n_{\text{GHD}})\|^2_\infty$ =?(?) μm^{-2}.

To determine x_0, we fit the expansion data at $\tau = 1$ ms with a model of a rectangular function convolved with a Gaussian, where x_0 is the center of the function. We obtain $x_0 = 5.5$ (18.4) μm. Next, we multiply the edge profile by a rectangular function centered

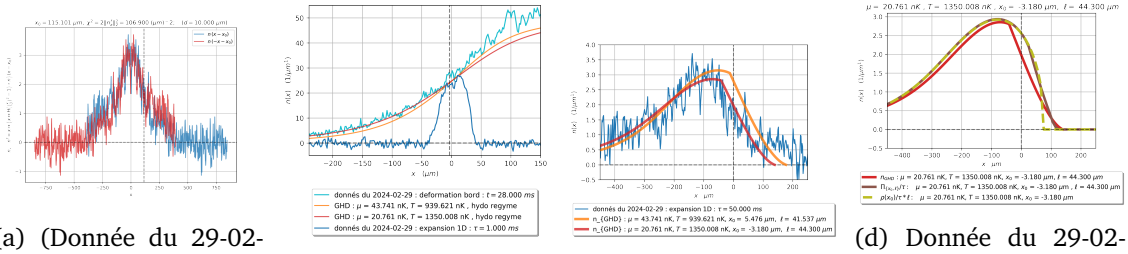

(a) (Donnée du 29-02-2024) (b) (c) (d) Donnée du 29-02-2024

Figure 3: Donnée du 29-02-2024

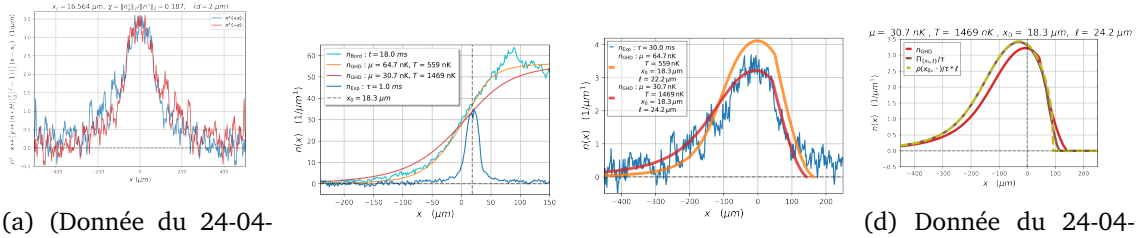

(a) (Donnée du 24-04-2024) (b) (c) (d) Donnée du 24-04-2024

Figure 4: Donnée du 24-04-2024

at x_0 with a diameter ℓ. We adjust ℓ to match the number of atoms in the slice to the one measured in the data at $\tau = 50$ (30) ms. This gives $\ell = 41.5$ (22.2) μm.

After the expansion, we observe an asymmetry in the data, with one side being steeper. This asymmetry is also visible in the GHD simulations $\tilde{n}_{\mathrm{GHD}}$, but differences are noticeable between the data and the GHD simulations, particularly on the non-thermal right-hand side. Over the interval $[-222, 70]$ ($[-150, 100]$) μm, $\chi^2 = \|(\tilde{n} - \tilde{n}_{\mathrm{GHD}})\|_\infty^2 = ?(?)$ (see orange curve in Fig. 4c). We consider increasing T and decreasing x_0.

We therefore performed a fit of the GHD simulations to the data after expansion. The fit was conducted with T and x_0 as adjustable parameters, while μ and ℓ retained the same constraints as previously described. The parameters obtained after this fit are $T = 1350$ (1000) nK and $x_0 = -3.18$ (17.8) μm (see red curve in Fig. 4c). Over the interval $[-222, 70]$ ($[-150, 100]$) μm, $\chi^2 = \|(\tilde{n} - \tilde{n}_{\mathrm{GHD}})\|_\infty^2 = ?(?)$ $\mu\mathrm{m}^{-2}$.

However, with these new parameters, the GHD simulations show less agreement with the edge deformation profiles. Over the interval $[-220, 70]$ ($[-150, 100]$) μm, $\chi^2 = \|(n - n_{\mathrm{GHD}})\|_\infty^2 = ?(?)$ $\mu\mathrm{m}^{-2}$ (see red curve in Fig. 4b). And even the x_0 ???.

Outside the interval $[-222, 70]$ ($[-150, 100]$) μm, we observe noise that is not explained by the GHD simulations.

The GHD simulations, already performed for a finite expansion time $\tau = 50$ (30) ms, are quite close to the predictions for $\tau^* \to \infty$, with $\ell \to 0$ being negligible, and the distribution $\rho_{x_0}/\tau * \ell$. The notable difference is a non-thermal vertical edge for $\rho_{x_0}/\tau * \ell$. For ℓ $\Pi_{x_0,\ell}/\tau$, as ℓ becomes non-negligible, the difference diminishes.

7 Conclusion

- a protocol that could enable the study of zero-entropy physics

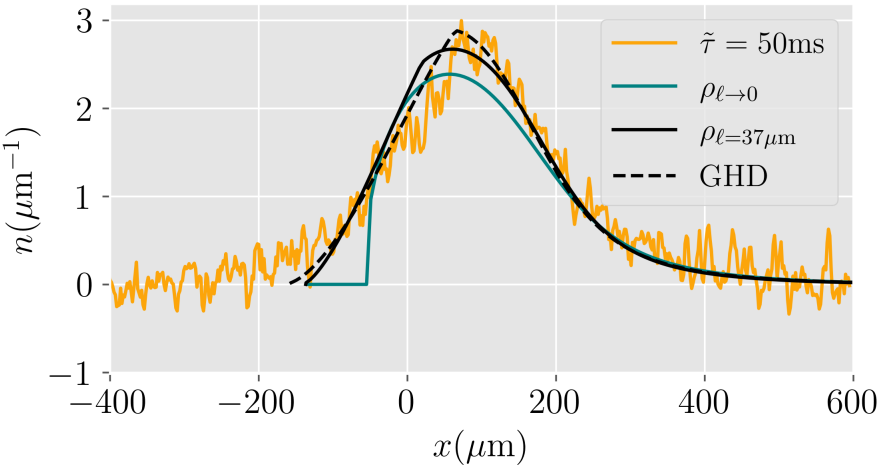

Figure 5: A second graph for this last part, change the format (.pdf). Add the profile n(-x) to add. Change the captions with using Π, the extensive rapidity distribution.

Acknowledgements

Funding information

A Details of calculations

Let us first introduce notations and usefull formulas. In the context of this paper, for an occupation factor distribution $\nu_0(\theta)$, we define the dressing as

$$f^{\rm dr}(\theta^*,\theta) = f(\theta) + \int_{-\infty}^{\theta^*} \frac{d\theta'}{2\pi}\Delta(\theta-\theta')\nu_0(\theta')f^{\rm dr}(\theta^*,\theta'). \tag{9}$$

The two following formulas are useful for our purposes:

- variation of a dressed quantity at 'Riemann point'

$$\frac{df^{\rm dr}(\theta^*,\theta^*)}{d\theta^*} = -\nu_0(\theta^*)f^{\rm dr}(\theta^*,\theta^*)\frac{[\Delta(.-\theta^*)]^{\rm dr}(\theta^*,\theta^*)}{2\pi} + f'(\theta^*) + \int_{-\infty}^{\theta^*}\Delta'(\theta^*-\theta')\nu_0(\theta')f^{\rm dr}(\theta^*,\theta')\frac{d\theta'}{2\pi}, \tag{10}$$

- variation of a charge density

$$\frac{d\left(\int_{\theta^*}^{\infty}\frac{d\theta}{2\pi}\nu_0(\theta)f^{\rm dr}(\theta^*,\theta)\right)}{d\theta^*} = -\nu_0(\theta^*)\frac{1^{\rm dr}(\theta^*,\theta^*)f^{\rm dr}(\theta^*,\theta^*)}{2\pi} \tag{11}$$

These formulas can be derived as follows. Varying the definition of the dressing (9) w.r.t θ^*, we get

$$\frac{d(f^{\rm dr}(\theta^*,\theta))}{d\theta^*} = -\nu_0(\theta^*)f^{\rm dr}(\theta^*,\theta^*)\frac{[\Delta(.-\theta^*)]^{\rm dr}(\theta^*,\theta)}{2\pi}.$$

Eq. (10) follows. Then the variation of the charge density is

$$\frac{d\left(\int_{-\infty}^{\theta^*}\frac{d\theta}{2\pi}\nu_0(\theta)f^{\rm dr}(\theta^*,\theta)\right)}{d\theta^*} = -\frac{1}{2\pi}\nu_0(\theta^*)f^{\rm dr}(\theta^*,\theta^*) - \nu_0(\theta^*)f^{\rm dr}(\theta^*,\theta^*)\int_{\theta^*}^{\infty}\frac{d\theta}{2\pi}\nu_0(\theta)\frac{[\Delta(.-\theta^*)]^{\rm dr}(\theta^*,\theta)}{2\pi}.$$

One then uses the fact that, for any functions g and h, $\int d\theta \nu(\theta) h^{\rm dr} g = \int d\theta \nu(\theta) h g^{\rm dr}$ to transform the integral in the r.h.s into $\int d\theta/(2\pi)\Delta(\theta-\theta^*)1^{\rm dr}(\theta^*,\theta)$. One then obtain formula (11).

Let us now derive Eq. (6). For simplicity let us denote $v^{\rm eff}(\theta^*)$ the quantity $v^{\rm eff}_{\nu^*}(\theta^*)$ where ν^* is defined Eq.3. Let us introduce $A(\theta^*) = dv^{\rm eff}/d\theta^*$. Using $v^{\rm eff} = \theta^{\rm dr}/1^{\rm dr}$ and using above formulas one finds

$$A(\theta^*) = \frac{1}{1^{\rm dr}(\theta^*,\theta^*)}\left(1+\int_{-\infty}^{\theta^*}\Delta'(\theta^*-\theta)[{\rm id}^{\rm dr}(\theta^*,\theta)-v^{\rm eff}(\theta^*)1^{\rm dr}(\theta^*,\theta)]\nu_0(\theta)\frac{d\theta}{2\pi}\right).$$

Let us now introduce $B(\theta^*)$ as $= B(\theta^*)\,\nu_0(\theta^*) = d(n(\theta^*))/d\theta^*$ where $n(\theta^*) = \int_{-\infty}^{\theta^*} d\theta \nu_0(\theta) 1^{\rm dr}(\theta^*,\theta)$ is the linear density for the occupation factor distribution ν^*. Using above formulas we obtain

$$B(\theta^*) = -\frac{1^{\rm dr}(\theta^*,\theta^*)^2}{2\pi}.$$

A discuter. A and B are functionals of ν_0 whose functional derivatives $\frac{\delta A}{\delta\nu(\theta)}$, $\frac{\delta B}{\delta\nu(\theta)}$, $\frac{\delta D}{\delta\nu(\theta)}$ are smooth at $\theta=\theta^*$. Let us now consider the border function $n(v)$ and the edge rapidity $\theta^*(v)$, defined in eq.4. Using $dn/dv = (dn/d\theta^*)(d\theta^*/dv)$ and the fact that $v = v^{\rm eff}(\theta^*)$, one finds

$$\nu(\theta^*) = \frac{A(\theta^*)}{B(\theta^*)}\frac{dn}{dv}. \tag{12}$$

Introducing $D = A/B$ and differentiating w.r.t θ^* this gives Eq. (6).

References

[1] B. Bertini, M. Collura, J. De Nardis and M. Fagotti, *Transport in Out-of-Equilibrium XXZ Chains: Exact Profiles of Charges and Currents*, Phys. Rev. Lett. **117**(20), 207201 (2016), doi:10.1103/PhysRevLett.117.207201.

[2] O. A. Castro-Alvaredo, B. Doyon and T. Yoshimura, *Emergent Hydrodynamics in Integrable Quantum Systems Out of Equilibrium*, Phys. Rev. X **6**(4), 041065 (2016), doi:10.1103/PhysRevX.6.041065.

[3] J. De Nardis, D. Bernard and B. Doyon, *Diffusion in generalized hydrodynamics and quasipaDiffusionrticle scattering*, SciPost Physics **6**(4), 049 (2019), doi:10.21468/SciPostPhys.6.4.049.

[4] J. De Nardis and M. Panfil, *Edge Singularities and Quasilong-Range Order in Nonequilibrium Steady States*, Phys. Rev. Lett. **120**(21), 217206 (2018), doi:10.1103/PhysRevLett.120.217206, Publisher: American Physical Society.

[5] E. H. Lieb and W. Liniger, *Exact Analysis of an Interacting Bose Gas. I. The General Solution and the Ground State*, Phys. Rev. **130**(4), 1605 (1963), doi:10.1103/PhysRev.130.1605.

[6] I. Bouchoule and J. Dubail, *Generalized hydrodynamics in the one-dimensional Bose gas: theory and experiments*, J. Stat. Mech. **2022**(1), 014003 (2022), doi:10.1088/1742-5468/ac3659.

[7] L. Dubois, G. Thémèze, F. Nogrette, J. Dubail and I. Bouchoule, *Probing the Local Rapidity Distribution of a One-Dimensional Bose Gas*, Phys. Rev. Lett. **133**(11), 113402 (2024), doi:10.1103/PhysRevLett.133.113402, Publisher: American Physical Society.

[8] J.-B. Trebbia, C. L. Garrido Alzar, R. Cornelussen, C. I. Westbrook and I. Bouchoule, *Roughness suppression via rapid current modulation on an atom chip*, Phys. Rev. Lett. **98**, 263201 (2007), doi:10.1103/PhysRevLett.98.263201.

[9] M. Olshanii, *Atomic scattering in the presence of an external confinement and a gas of impenetrable bosons*, Phys. Rev. Lett. **81**, 938 (1998), doi:10.1103/PhysRevLett.81.938.

[10] K. V. Kheruntsyan, D. M. Gangardt, P. D. Drummond and G. V. Shlyapnikov, *Pair correlations in a finite-temperature 1d bose gas*, Phys. Rev. Lett. **91**, 040403 (2003), doi:10.1103/PhysRevLett.91.040403.

[11] L. Dubois, G. Thémèze, F. Nogrette, J. Dubail and I. Bouchoule, *Probing the local rapidity distribution of a one-dimensional bose gas*, Phys. Rev. Lett. **133**, 113402 (2024), doi:10.1103/PhysRevLett.133.113402.

[12] M. Girardeau, *Relationship between Systems of Impenetrable Bosons and Fermions in One Dimension*, Journal of Mathematical Physics **1**(6), 516 (1960), doi:10.1063/1.1703687.

[13] G. A. El, V. V. Geogjaev, A. V. Gurevich and A. L. Krylov, *Decay of an initial discontinuity in the defocusing NLS hydrodynamics*, Physica D: Nonlinear Phenomena **87**(1), 186 (1995), doi:10.1016/0167-2789(95)00147-V.

[14] G. Xu, M. Conforti, A. Kudlinski, A. Mussot and S. Trillo, *Dispersive dam-break flow of a photon fluid*, Phys. Rev. Lett. **118**(25), 254101 (2017), doi:10.1103/PhysRevLett.118.254101, ArXiv:1703.09019 [nlin, physics:physics].